A Data-Driven Case Generation Model for Transient Stability Assessment Using Generative Adversarial Networks

Jiashu Fang, *Member, IEEE*, Le Zheng, *Member, IEEE*, Chongru Liu, *Senior Member, IEEE*, and Chenbo Su

***Abstract*—Online transient stability assessment (TSA) is crucial for ensuring the security of modern grids. However, problems with limited sample sizes and data imbalance hinder the performance of data-driven TSA classifiers. Addressing this challenge, this article presents a generative adversarial network (GAN)-based model to generate instability samples. Unlike existing methods, our approach moderately alters the long-tailed distribution of instability moments within the raw dataset, producing a more diverse database for TSA tasks. A convolutional neural network-based supervised model, mapping the relationship between fault-clearance electrical characteristics and instability moments of the power system, is incorporated to drive the GAN model to generate realistic yet rare instability cases. Numerical results have proven the superiority of the proposed model over existing case generation methods in terms of realistic and diverse sample generation. In addition, the effectiveness of the proposed data augmentation scheme is demonstrated for online TSA applications.**

***Index Terms*—Case generation, generative adversarial networks (GANs), power system, transition stability assessment (TSA).**

I. Introduction

THE reliable and efficient online transient stability assessment (TSA) is critical to ensure the security of modern power systems, particularly with the increased integration of intermittent renewable energy sources and power electronic components. Various data-driven models (e.g., [1], [2], [3]) have been proposed to predict the transient stability. However, the scarcity of unstable samples in the training set constrains the performance of data-driven TSA classifiers [4], [5]. To overcome issues related to data imbalance and small sample sizes, data augmentation methods are required to generate realistic instability samples for data-driven TSA methods.

Received 18 December 2023; revised 22 July 2024; accepted 8 August 2024. Date of publication 16 September 2024; date of current version 5 December 2024. This work was supported by the National Natural Science Foundation of China under Grant U23B6008. Paper no. TII-23-5120. *(Corresponding authors: Chongru Liu; Chenbo Su.)*

Jiashu Fang was with the State Key Laboratory of Alternate Electrical Power System with Renewable Energy Sources, North China Electric Power University, Beijing 102206, China. She is now with the University of Electronic Science and Technology of China, Chengdu 611731, China.

Le Zheng and Chongru Liu are with the State Key Laboratory of Alternate Electrical Power System with Renewable Energy Sources, North China Electric Power University, Beijing 102206, China (e-mail: chongru.liu@ncepu.edu.cn).

Chenbo Su is with the State Key Lab of Power Systems, Department of Electrical Engineering, Tsinghua University, Beijing 100084, China (e-mail: scb2636@foxmail.com).

Color versions of one or more figures in this article are available at https://doi.org/10.1109/TII.2024.3452211.

Digital Object Identifier 10.1109/TII.2024.3452211

Given this challenge, various data augmentation methods have been proposed in literature. Conventional methods involve constructing a balanced dataset through repetition, synthesis, or deletion of samples. Gupta et al. [3] utilized subsampling to ensure an equal number of all classes in the training dataset. Douzas et al. [6] presented an oversampling method, which leverages k-means clustering and synthetic minority oversampling technique to address imbalances between classes. However, subsampling would result in underfitting due to the loss of patterns. Moreover, these oversampling methods, relying on linear interpolation of minority data [7], are inadequate for capturing the complex interactions within the power system, which comprises numerous nonlinear devices [8].

To address the aforementioned issues, data generation techniques based on the deep learning approach, specifically generative adversarial networks (GANs), are motivated. GANs have shown potential in learning complex distributions from raw datasets in power systems and generating realistic samples [4], [9], [10], [11], [12], [13], [14], [15], [16]. Zhu and Hill [4] generated samples through cycle generative adversarial networks (CycleGANs) to solve the small sample size and class imbalance issues in historical databases. Yuan et al. [10] employed a style-based GAN and a sequence encoder network, incorporating different-level scenario style control and mixing to enhance the characterization of renewable spatial-temporal dynamics. Chen et al. [14] proposed a GAN-based model for generating renewable resource scenarios that adhere to the same distribution as historical data. Li et al. [15] utilized a Wasserstein deep convolutional GAN (DCGAN), effectively balancing data usability and privacy levels through a hyperparameter set during training. The high performance across different classifiers attests to the desired diversity and realism of the generated data. Chhetri et al. [16] adopted a conditional GAN-based approach, modeling the conditional probability distribution among various information flows. Dong et al. [17] proposed a controllable GAN model with interpretability for the renewable scenario generation task. Liu et al. [18] incorporated the attention mechanism and spectral normalization to stabilize the training process in cases of small sample sizes.

Conventional GAN-based methods typically generate unstable samples closely resembling the original dataset. However, as suggested by existing literature [19], TSA classifiers are hard to recognize the instability samples with prolonged instability moments due to the less evident unstable characteristics and scarcity of such samples in the raw training set. Consequently, there is a motivation to create a distribution-shifted dataset with an increased number of samples featuring prolonged instability moments compared to the original dataset, enhancing the training of the TSA classifier.

Considering the existing research gap, this article develops a GAN-based model to generate a diverse range of realistic instability samples, gradually shifting the generated data distribution in the direction of fitting the tail of the distribution. To achieve this, the instability moment of a sample is used as the index to indicate different instability states. A well-designed convolutional neural network (CNN)-based regression model is built to map the relationship between the electrical measurements at the fault clearance moment and instability moments of the power system. This CNN model is integrated into the GAN structure, incorporating the instability characteristics as additional knowledge, to drive the GAN model to generate realistic yet rare instability scenarios from the raw database. As a practical application, the effectiveness of the proposed GAN-based method as a data augmentation tool has been demonstrated for various TSA classifiers. To the best of our knowledge, this is the first time a case generation model is proposed to generate a sample set including more diverse scenarios, rather than drawing data from the bulk of the raw distribution.

The main contributions of this article include the following.

1) To address the challenges of small sample size and data imbalance in existing datasets, a GAN-based case generation method is proposed to expand the basic sample set for TSA tasks.
2) Unlike conventional GAN-based models, the proposed method introduces a modified loss function, which converts the long-tailed distribution in the raw training set into a more moderate distribution. This function introduces additional instances with prolonged instability moments into the training set of the TSA classifier, thereby improving the classification performance.
3) Addressing the challenge of obtaining instability moments directly from signals in complex power systems, a supervised CNN-based model, which maps the relationship between current measurements and instability moments, is constructed and integrated into the GAN structure. This, combined with the modified loss function, ensures the generation of specific training samples tailored for TSA classification tasks.

The rest of this article is organized as follows. The proposed algorithm is elaborated in Section II. In Section III, the realism of the generated cases is analyzed in terms of distance metrics and correlation coefficients within feature maps, and the case generation performance is compared versus existing approaches. Section IV demonstrates the effectiveness of the proposed data augmentation approach for an online TSA task. The model's effectiveness in a large-scale power system with limited data is demonstrated in Section V. Finally, Section VI concludes this article.

II. Proposed Case Generation Approach

In this section, a novel GAN-based model is designed to generate unstable samples that address the challenges of small sample size and class imbalance in TSA tasks. Unlike existing data augmentation methods that generate samples with long-tailed distributions similar to the raw data, the proposed GAN model generates data with a shifted yet moderate distribution.

A. Proposed Model Overview

A GAN-based algorithm is constructed with two deep neural networks, denoted as the generator G and the discriminator D to learn high-dimensional distributions. D and G play a two-player minimax game with value function $V(G,D)$, and the overall objective of GAN can be defined as

$$\min_G \max_D V(D,G) = \mathbb{E}_{x\sim P_{\text{data}}(x)}[\log D(\boldsymbol{x})] + \mathbb{E}_{z\sim P_z(z)}[\log(1 - D(G(\boldsymbol{z})))] \quad (1)$$

where $P_{\text{data}}(x)$ and $P_z(z)$ denote the real and noise data distributions, respectively, with $\mathbb{E}$ indicating the expectation. The generator produces data samples from a noise distribution $P_z(z)$, and the discriminator evaluates these samples and provides feedback to the generator. The generator is trained to generate increasingly realistic data samples that are more difficult to distinguish from the original data. The confrontational training improves the performance of both G and D.

B. Discriminator

The discriminator D takes the generated matrix $G(\boldsymbol{z})$ as input. As described in (1), the discriminator aims to maximize the probability for real samples and minimize the probability for fake samples, differentiating between original (true) data x and generated (fake) data $G(\boldsymbol{z})$. To address the potential gradient vanishing issue in GAN learning, the logarithmic losses in (1) are replaced with square losses [20] as

$$\max_D \mathcal{L}_D = \mathbb{E}_{x\sim P_{\text{data}}(x)}\left[(D(\boldsymbol{x}))^2\right] + \mathbb{E}_{z\sim P_z(z)}\left[1 - D(G(\boldsymbol{z}))^2\right]. \quad (2)$$

To enhance stability and efficiency in GAN training, the maximization problem transforms into a minimization problem as

$$\min_D \mathcal{L}_D = \mathbb{E}_{x\sim P_{\text{data}}(x)}\left[(D(\boldsymbol{x}) - 1)^2\right] + \mathbb{E}_{z\sim P_z(z)}\left[D(G(\boldsymbol{z}))^2\right]. \quad (3)$$

C. Generator

The generator G takes the noise matrix $\mathbf{Z}$ as input. $\mathbf{Z} \in \mathbb{R}^{d\times c}$ is a prior defined on input noise variables to learn the generator's distribution over the true data matrix $\mathbf{X}$. d and c are, respectively, the number of phasor measurement units (PMUs) and the number of electrical variable measurements. The loss $\mathcal{L}_G$ in the generator evaluates the generator's ability to generate realistic data, as indicated in (1). To this end, the benchmark model writes

$$\min_G \mathcal{L}_G^{\text{benchmark}} = \mathbb{E}_{z\sim P_z(z)}\left[(D(G(\boldsymbol{z})) - 1)^2\right]. \quad (4)$$

TABLE I
DETAILS OF THE GENERATOR

Layer	Description
ConvTranspose$_1$ InstanceNorm$_1$ LeakyReLU	40 filters, size=1, stride=1 negative slope=0.2
ConvTranspose$_2$ tanh	1 filter, size=1, stride=1

TABLE II
DETAILS OF THE DISCRIMINATOR

Layer	Description
Conv$_1$ InstanceNorm$_1$ LeakyReLU	32 filters, size=2, stride=1 negative slope=0.2
Conv$_2$ InstanceNorm$_2$ LeakyReLU	64 filters, size=2, stride=1 negative slope=0.2
Conv$_2$ InstanceNorm$_3$ LeakyReLU	128 filters, size=2, stride=1 negative slope=0.2
Conv$_3$ Sigmoid	16 filter, size=2, stride=1

Overall, (1) represents the adversarial interaction between the generator and the discriminator. Specifically, the objectives of the discriminator and generator are, respectively, guided by (3) and (4) in conventional GANs. The output of the discriminator is in the range [0,1] due to the sigmoid activation function, as demonstrated in Table II. This adversarial process encourages the generator to produce more realistic samples.

In conventional GANs, the generated samples usually resemble the distribution of the original data. However, apart from generating realistic samples, in this study, we seek to produce samples with a distinct distribution, specifically generating more instances with extended instability moments. These instances were rare in the raw dataset, making them challenging for TSA identification, as emphasized in [19].

To address this, unlike the conventional generator loss [$\mathcal{L}_G^{\text{benchmark}}$ in (4)], we introduce a two-part loss function into the generator. The objective of G considers both sample realism and the shifted distribution of instability moments, and is given by

$$\min_G \mathcal{L}_G = \mathcal{L}_G^{\text{benchmark}}(\boldsymbol{z}) + \alpha \mathcal{L}_M(\boldsymbol{z}) \tag{5}$$

where α is a hyperparameter (set to 0.7 in this article via cross validation). Thus, the objectives of the discriminator and generator are separately guided by (3) and (5).

To facilitate the generation of numerous samples with prolonged instability moments, loss $\mathcal{L}_M$ in (5) is designed to evaluate the distance between the average instability moments of generated samples and the maximum instability moments from the raw data, leading to a shifted distribution of instability moments in generated samples w.r.t. the raw dataset. This gives

$$\min_G \mathcal{L}_M = \left| \frac{1}{m} \sum_i^m C\left(G\left(\boldsymbol{z}\right)\right) - \max_i^m C\left(\boldsymbol{x}\right) \right|^2 \tag{6}$$

where m is the number of unstable samples. Equation (6) acts as a penalty in the data generation process, and encourages generating samples with extended instability moments as G iteratively evolves.

Due to the complexity of power system characteristics that hinders directly obtaining instability moments from samples, the proposed method first involves training a fitting model C based on the samples and their corresponding instability moments, as illustrated in Fig. 1 and detailed in Section III-A. Once this fitting model C is trained, its internal parameters are no longer updated. Consequently, $\max_i^m C(\boldsymbol{x})$ remains constant during the GAN network training with fixed internal parameters in model C and the original data $\boldsymbol{x}$. After training the model C, in the second step of the proposed method, the trained model C with fixed parameters is integrated into the GAN structure as a function to accurately assess the instability moments of the generated cases $G(\boldsymbol{z})$.

To prevent overfitting, an early stopping technique is employed to monitor the performance of the model on the testing set and stop the training process when $\mathcal{L}_G$ starts to increase, thereby guaranteeing the model to generate samples that are highly similar to the original ones.

Aiming at minimizing the prediction errors in the proposed regression model C, its learning objective is described as

$$\min \mathcal{L}_C = \sqrt{\frac{1}{n} \cdot \sum\nolimits_{i=1}^{n} \left|\hat{\mathrm{x}}_i - \mathrm{x}_i\right|^2} \tag{7}$$

where n is the number of unstable samples, and $\hat{x_i}$ and x_i are, respectively, the predicted and true instability moments.

III. Numerical Results and Analysis

In this section, the performance of the proposed model is discussed with numerical experiments. Section III-A introduces the database utilized in this article; Section III-B demonstrates model performance and discusses the effect of each modified block in the algorithm; Section III-C illustrates the realism of the generated cases in terms of inherent spatial correlations in the power system; finally, Section III-D not only shows the higher realism achieved by the proposed model compared to existing approaches but also presents the high sample diversity provided by the proposed method, highlighted by the more uniformly distributed instability moments of the generated samples.

A. Database Generation

Databases are generated by simulating various operational conditions and contingencies based on a 50-Hz IEEE-39 power system. The proposed method serves as a preliminary data processing step for the TSA model, and therefore, the sample space of the proposed GAN-based approach is aligned with that of the existing TSA classifier model, ensuring that the operation range of the power system and the baseline operating point are consistent. A feature map, denoted as $\mathbf{Z} \in \mathbb{R}^{d \times c}$, is employed to capture the spatial dynamics of the power system. It represents d electrical variables recorded by various PMUs located in c generators at the moment of fault clearance. In this study, we set d to 3 and c to 10, corresponding to the electrical variables, including active power, voltage magnitude, and phase angle, of a total of ten generators in the IEEE-39 power system.

To ensure sufficient diversity between operating points within the database, various fault conditions and operating points are

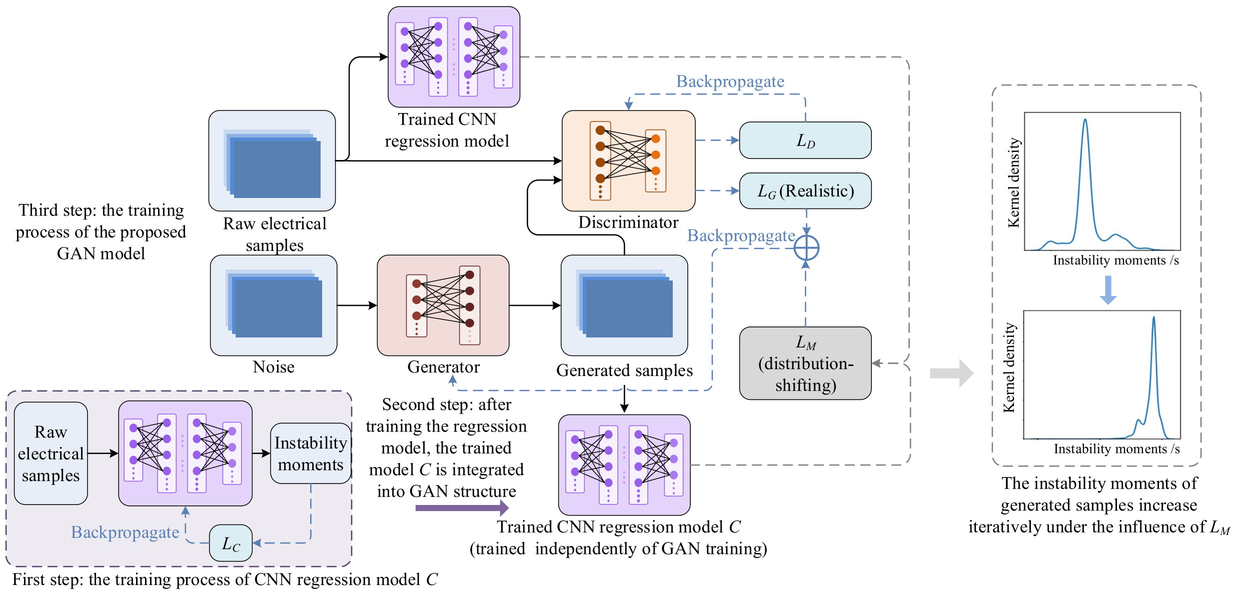

Fig. 1. Training process of the proposed method.

considered. Specifically, the loads in power systems are randomly determined with the generation gradually decreasing from 120% to 80% of the basic operating level [19]. The bus voltage is maintained within the range of 0.95–1.05 p.u. Moreover, three phase-to-ground short-circuit faults are applied at three different locations (25%, 50%, and 70% of the length) [21]. The transient stability simulations are conducted using Power System Toolbox 3.0 [22], and the simulation period is set to 10 s. In total, 12 000 scenarios are generated, including 4068 unstable scenarios.

To determine if a sample is stable or not, the transient stability index (TSI) is used as the stability criterion [19], yielding

$$\mathrm{TSI} = \frac{360^\circ - |\Delta\delta_{\max}|}{360^\circ + |\Delta\delta_{\max}|} \tag{8}$$

where $|\Delta\delta_{\max}|$ is the absolute value of the maximum separation angle between any two generators. When TSI > 0 the system is considered stable and vice versa. It is noted that only 3000 raw unstable cases are used to train the proposed model C that maps the relationship between electrical characteristics and instability moments. Similarly, the proposed GAN-based model employs only raw unstable cases to generate additional instances, as the stable samples widely exist in historical records, in contrast to the scarcity of unstable ones.

B. Performance of Proposed Model

The architecture of the GAN is carefully designed, as shown in Tables I and II. The rationale behind the architecture design is to use a relatively simple model structure with fewer parameters. The proposed GAN model and the integrated regression model C are designed based on CNN architecture, inspired by the resemblance of spatial relationships within power system buses to the data structure of images [19]. Consequently, CNN, widely used for image classification, is motivated for extracting the complex spatial dependencies within the power system. In this study, we utilize a convolutional transpose (ConvTranspose) operation with a kernel size of 1 in the generator, instead of the conventional use of higher resolution and larger kernel sizes in GAN generators for feature map generation. The rationale behind this choice is rooted in the task of generating samples for TSA. Specifically, each variable in the electrical samples contains distinct power generator information, and the relationships among different generators determine power system stability, as indicated in (8). Thus, this structure enables the generator to precisely preserve information at the pixel level. This is crucial for accurately depicting the dynamic characteristics of the power system in the generated samples.

TABLE III
PERFORMANCE OF GAN MODEL WITH DIFFERENT COMPONENTS

Training data	Conv	InstanceNorm	LeakyReLU	FID
Without pollution	✓		✓	0.1375
		✓	✓	0.1291
	✓	✓		0.1250
	✓	✓	✓	0.0749
With pollution	✓		✓	0.2728
		✓	✓	0.2015
	✓	✓		0.1613
	✓	✓	✓	0.1075

The performance of the proposed generator is evaluated using the Fréchet inception distance (FID) metric [23], which compares the distributions of real and generated samples based on the activation distributions of the final layer, yielding

$$\mathrm{FID} = \|\mu_r - \mu_g\|_2^2 + \mathrm{tr}\,(\Sigma_r) + \mathrm{tr}\,(\Sigma_g) - 2\cdot\mathrm{tr}\left(\sqrt{\Sigma_r\Sigma_g}\right) \tag{9}$$

where tr denotes the trace of a matrix. (μ_r, Σ_r) and (μ_g, Σ_g) are the mean–covariance pairs of the real and generated distributions, respectively.

In order to investigate the contribution of model components on the overall GAN performance, Table III demonstrates FID scores of different model structures obtained via the removal of specific components. Two scenarios are considered. Initially, direct data with unstable simulation cases are selected as training data (i.e., without pollution case in Table III). Besides, considering the feasibility of directly establishing the data generation method based on PMU historical data [19], we introduced noise and random data missing into the training dataset (i.e., with pollution case in Table III) to assess the model's robustness against common field pollution in PMU records. In the latter case, the measurement noise is lower than 1% of its actual value, and the missing rate is set at 10%, following the IEEE Standard [24] and informed by historical operational data from China's power grid [25]. In both cases, the FID score compares the generated samples with the pollution-free samples. Indeed, for the latter case, as pollution was added afterward, initial pollution-free samples are available from the simulation. This ensures that the result accurately reflects the similarity between the generated samples and the authentic dynamic responses of the power system. Note that the removal of the convolution module in Table III is only tested in the discriminator to preserve the dimensions of samples in generators.

As shown in Table III, the InstanceNorm [26] was utilized to reduce the internal covariate shift and achieve more stable training dynamics. The results show that the removal of the InstanceNorm led to a decrease in the model's ability to generate highly realistic cases. In addition, the absence of the leaky rectified linear unit (LeakyReLU), which was introduced to avoid the zero-gradient problem in the standard ReLU function and provide faster convergence during the training process [27], obviously decreases the model performance. Overall, Table III illustrates the improved performance under pollution-free and field training data, highlighting the importance of the proposed model structure in achieving better results for extracting electrical characteristics and generating realistic samples.

Further, as depicted by (5) and (6), a regression model that can accurately predict instability moments, particularly for samples with prolonged instability moments, is crucial for the completion of the proposed case generation model. The regression model performance is evaluated by the mean absolute percentage error (MAPE) between the real and predicted instability moments as

$$\mathrm{MAPE} = \frac{1}{N} \cdot \sum_{i=1}^{N} \left| \frac{\hat{\mathrm{x}}_i - \mathrm{x}_i}{\mathrm{x}_i} \right| \times 100\% \tag{10}$$

where N is the number of unstable samples, and $\hat{x}_i$ and x_i are, respectively, the predicted and true instability moments.

The proposed regression component is constructed utilizing several components (see Table IV), including convolutional layers (Convs), nonlocal blocks, and residual blocks (Resblock) [28]. Table V indicates the contribution of each model component for the regression task. The results indicate that both the Resblock and the nonlocal block improve the performance of the model. The attention mechanism introduced by nonlocal modules contributes to improving the model performance. In this study, each variable in the electrical samples represents specific power system generator node information, and the difference in electrical variables between generators correlates with the instability moment. Consequently, the generator information determining instability moments may not be in adjacent positions in the feature map. The attention computation facilitates the interaction of electrical information regardless of relative distances within the feature map [29]. In addition, accurately predicting the instability moments becomes more challenging with field PMU measurements pollution. The incorporation of attention in the nonlocal module significantly improves the model's accuracy. In particular, when part of the node information is missing, the attention computation in the nonlocal block encourages the model to extract information from positions with available information [29], thereby enhancing the model's robustness to predict instability moments.

TABLE IV
DETAILS OF THE REGRESSION MODEL C

Layer	Description
Conv_1 Pool_1	[32 filters, size=3, ReLU] $\times$ 2 max-pooling, size=2
$\mathrm{ResBlock}_2$ Pool_2 $\mathrm{Non\text{-}local}_2$	[64 filters, size=3, ReLU] $\times$ 2 max-pooling, size=2 C'=32
$\mathrm{ResBlock}_3$ Pool_3 $\mathrm{Non\text{-}local}_3$	[128 filters, size=3, ReLU] $\times$ 2 max-pooling, size=2 C'=64
Fully connected Fully connected Fully connected	kernel number=64 kernel number=32 kernel number=1

TABLE V
PERFORMANCE OF MODEL C WITH DIFFERENT COMPONENTS

Training data	Conv	ResBlock	Nonlocal	MAPE (%)
Without pollution	✓			3.32
		✓	✓	2.38
	✓	✓		1.62
	✓	✓	✓	0.94
With pollution	✓			3.51
		✓	✓	2.42
	✓	✓		1.81
	✓	✓	✓	0.99

TABLE VI
REALISM LEVEL OF CRITICAL INSTABILITY SAMPLES GENERATED BY MODELS WITH/WITHOUT REGRESSION COMPONENT C EMBEDDED

Method	FID (rare scenarios)	FID (all scenarios)
Model with C	0.0820	0.0749
Model without C	0.2995	0.1120

The supervised regression component C is employed to establish the correlation between instability moments and electrical variables, as shown in Fig. 1. To assess the effectiveness of the combined model C in generating high-quality instability samples, Table VI compares the FID (lower is better) between real and generated samples. Since the goal of this study is to generate a database that mitigates the long-tailed distribution, we focused on evaluating the realism level of rare scenarios in the raw dataset with instability moments greater than 4 s, which accounted for only 17% of the original instability dataset but are critical for TSA tasks.

The results in Table VI indicate that the combination of C enhances the overall realism level of generated cases, and the injection of additional instability knowledge, introduced via the model C, improves the GAN's ability to produce highly realistic scenarios. Moreover, the proposed approach gradually shifts the data distribution in the direction of increasing rare

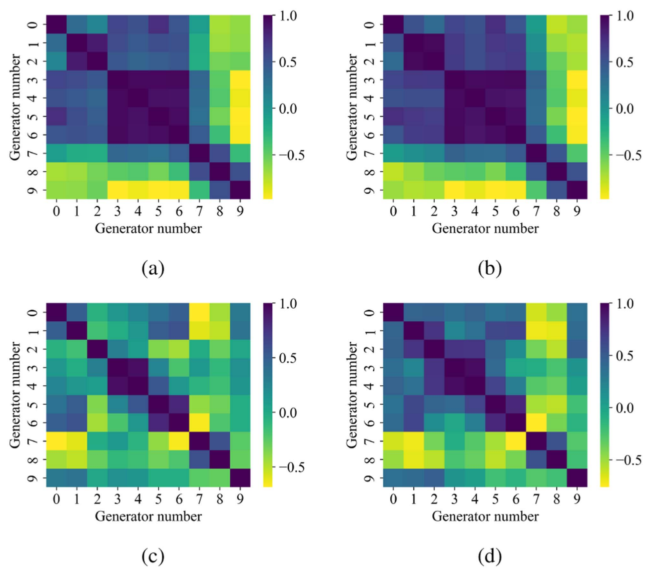

Fig. 2. Correlations among multiple variables in original and generated samples. (a) and (b) Correlations among phase angles of different generators in original and generated cases, respectively. (c) and (d) Correlations among voltage magnitudes of different generators in original and generated cases, respectively.

scenarios by utilizing $\mathcal{L}_G$ in (6). This strategy enables the GAN model to progressively fit the tail of the distribution, rather than the bulk, thereby enhancing the model's ability to generate highly realistic tail cases within the distribution. Therefore, the proposed method allows the generator G to produce realistic scenarios, particularly those that are rare in the original dataset.

C. Correlation Analysis of the Generated Cases

This section aims to prove the realism of the generated cases. Specifically, correlation analysis is performed to evaluate whether the proposed model can maintain the inherent spatial-temporal relationships regarding each electrical variable. Therefore, thissection demonstrates that similar correlations exist among individual buses in the generated and raw samples of the power grid. The correlation coefficient is calculated as [30]

$$\mathbf{r}(\mathbf{x}, \mathbf{y}) = \frac{\sum_{j=1}^{k} (x_j - \bar{x})(y_j - \bar{y})}{\sqrt{\sum_{j=1}^{k} (x_j - \bar{x})^2 \sum_{j=1}^{k} (y_j - \bar{y})^2}} \tag{11}$$

where $\bar{x}$ and $\bar{y}$ are the sample means of electrical variables x and y. $\mathbf{r}(\mathbf{x}, \mathbf{y})$ measures the relative correlation of bus j to remaining buses in the power system.

Fig. 2 displays the correlations in the original and the generated cases. The high similarity between them suggests that the proposed method can effectively capture the underlying spatial-temporal correlations present in the original cases, which reflect the physical constraints of the power system. In addition, the correlations regarding angles exhibit a higher similarity compared to those regarding voltage magnitudes. This observation can be attributed to the criterion for determining transient stability of a power system being based on the angles of generators, causing the proposed model to primarily focus on learning the distribution of angles rather than of voltage magnitudes.

TABLE VII
REALISM LEVEL OF UNSTABLE SAMPLES GENERATED BY DIFFERENT MODELS

Method	FID (rare scenarios)	FID (all scenarios)
Proposed algorithm	0.0820	0.0749
DCGAN [13]	0.3082	0.1248
cGAN [31]	0.3924	0.1258
VAE [33]	0.4501	0.1332
DDPM [32]	0.3131	0.0981

D. Comparison Versus Existing Data Augmentation Approaches

To assess the effectiveness of our proposed method, we conduct a comprehensive comparison of model performance, focusing on both the realism and diversity of the generated cases. The proposed model is compared to commonly used data augmentation techniques, including DCGAN [13], cross-modal GAN (cGAN) [31] based on attention computation, residual UNet-based denoising diffusion probabilistic model (DDPM) [32], and CNN-based variational autoencoder (VAE) [33]. Grid search is used to determine the optimal hyperparameters of models.

For realism comparison, FID scores of different methods are shown in Table VII. cGAN, VAE, and DDPM exhibit higher FID scores, indicating a less accurate representation of rare instability scenarios and the overall power system dynamics. In addition, the noticeably high FID scores in rare scenarios for the comparative models suggest their reduced ability to generate samples that correspond to scenarios occurring less frequently in the original dataset. The highly uneven distribution in the raw dataset causes these comparative models to draw information from the bulk of the distribution, lacking sufficient extraction of rarely seen power system scenarios at the tail of the dataset. Conversely, the proposed GAN model, designed specifically for generating power system samples with rare instability scenarios, achieves the highest realism level compared to other existing models. This indicates that the proposed GAN model excels in capturing spatial dependencies and complex patterns in the power system.

The dataset diversity for TSA tasks is reflected in the instability moment distributions. Fig. 3 illustrates the training datasets under a line 19–33 fault. In Fig. 3(c), RGB plots of samples with ascending instability moments are displayed. The RGB channels correspond to three distinct electrical parameters at the fault clearance moment, as explained in Section III-A. The visualization reveals a noticeable regular change in the power system's dynamic response with increased instability moments, supporting the feasibility of constructing a regression model C to capture the relationship between samples and their corresponding instability moments. In addition, to demonstrate the enhanced TSA performance introduced by the proposed method, the training set employed in this study is consistent with existing data-driven TSA methods [19]. Fig. 3(d) illustrates a distinct long-tailed distribution of the instability moments within the raw data. Samples with prolonged instability moments are situated in the tail of the distribution, representing rare occurrences in the raw dataset. It is worth noting that the prolonged instability moments suggest that the unstable characteristics at the fault clearance moment are less apparent for recognition by TSA classifiers. The scarcity of such scenarios in the raw data further diminishes the TSA classifiers' ability to effectively identify

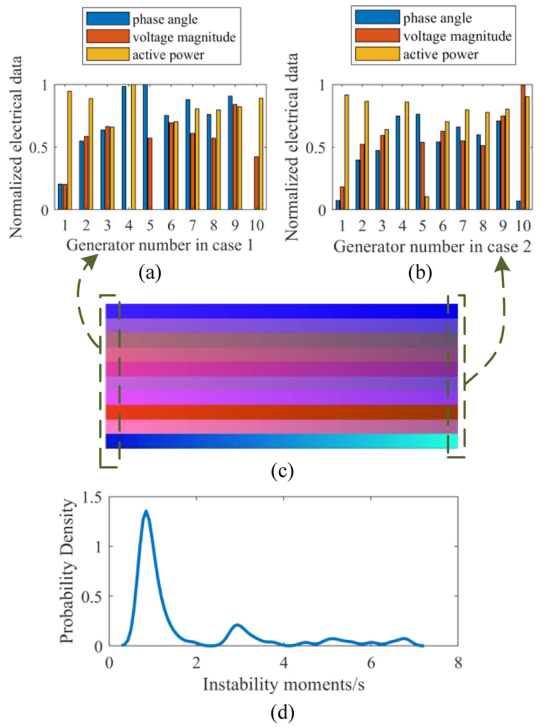

Fig. 3. (a) Sample at fault clearance, losing stability 0.72 s later, i.e., with an instability moment of 0.72 s. (b) Sample with an instability moment of 6.74 s. (c) RGB visualization of samples sorted by instability moment growth under the line 19–33 fault. (d) Long-tailed distribution of instability moments for samples in (c).

such occurrences. To provide specific examples, Case 1 in Fig. 3(a) illustrates the generator variables at the fault clearance moment. In this case, the power system exhibits the so-called aperiodic instability with a short instability moment, where the system loses synchronism during the first or second swing [as depicted in Fig. 4(a)]. In contrast, Case 2 in Fig. 3(b) displays an oscillatory instability sample with prolonged power system instability moment [as shown in Fig. 4(b)].

To evaluate dataset diversity in TSA tasks, we compare the distribution of instability moments among datasets generated by existing methods. Fig. 3(c) illustrates that various electrical dynamic states result in different corresponding instability moments, indicating that higher diversity in TSA tasks can be inferred from a more uniform distribution of instability moments. Fig. 4 illustrates the distribution of instability moments within various generated datasets, providing evidence for the increased diversity of the augmented dataset through the proposed data generation method. In particular, compared to other algorithms, VAE generates data with very few instability moments exceeding 6 s, suggesting its limited capability in generating diverse samples. Moreover, the data distribution generated by DCGAN is most similar to the original data, which proves the effectiveness of convolutional operations in reproducing power grid data. As shown in Fig. 4(c)–(f), the instability moments generated by the reference methods are in close alignment with the raw database, and the majority of the generated cases have instability moments within 4 s. However, as depicted in Fig. 4(g), significant changes in terms of instability moments can be observed for the proposed method in comparison to other approaches. The proposed loss function (6) has shifted the distribution toward

TABLE VIII
ACCURACY OF DIFFERENT TSA CLASSIFIERS WITH DIFFERENT TRAINING DATASETS

Test data	Training data	Classifiers (%)		
		CNN	SVM	DBN
Without pollution	Raw data	98.08	97.15	97.54
	Augmented - DCGAN	98.25	97.22	97.58
	Augmented - proposed method	99.73	97.33	97.98
With pollution	Raw data	97.61	95.76	97.01
	Augmented - DCGAN	98.01	96.10	97.32
	Augmented - proposed method	99.67	96.28	97.85

generating more tail data with prolonged instability moments. Therefore, compared to the original database, the database generated by the proposed method presents higher diversity with more uniformly distributed instability moments.

IV. Application to Online TSA

The increased integration of renewable energy sources and power electronic components in modern power systems has posed challenges to TSA using conventional approaches. Therefore, data-driven TSA methods are proposed to provide accurate assessments of transient stability [2], [19], [34]. The feature map in the TSA classifier is consistent with the proposed GAN model, as detailed in Section III-A.

To further demonstrate the advantage of the proposed case generation framework in enhancing the online TSA performance, various data schemes are used to train three classical classification TSA models, including CNN [19], support vector machine (SVM) [2], and deep belief network (DBN) [34]. Two augmentation methods, DCGAN and the proposed model, are employed independently, each producing an addition of 4000 unstable samples, thus resulting in an approximately balanced ratio of stable and unstable samples in the training set, as mentioned in Section III-A. Classification results are presented on the original testing set, considering scenarios with and without PMU field measurement pollution.

Table VIII reveals that classification accuracy drops when data augmentation is absent. In this case, the imbalanced numbers of stable and unstable instances in the dataset result in underfitting of unstable instances and a bias toward identifying unknown instances as stable. DCGAN-based data augmentation marginally enhances TSA performance. Conversely, the data augmentation technique proposed in this study results in a significant improvement in classification performance. Moreover, it can be observed that the introduction of field pollution reduces the accuracy of the TSA classifier. Nevertheless, the TSA classifier, trained on an improved dataset using the proposed algorithm, exhibits heightened robustness. This can be attributed to the improved sample diversity, characterized by a substantial increase in the proportion of unstable samples with longer instability moments in the training set, as depicted in Fig. 4(g). Models trained on these augmented samples exhibit superior performance in recognizing early signals of instability. This proves the necessity of the proposed approach in practical applications of TSA.

To substantiate the effectiveness of the proposed algorithm for the performance improvement of the TSA classifier, the prediction probability of the classifier, which reflects the confidence level of the classifier in its prediction [35], is computed using the

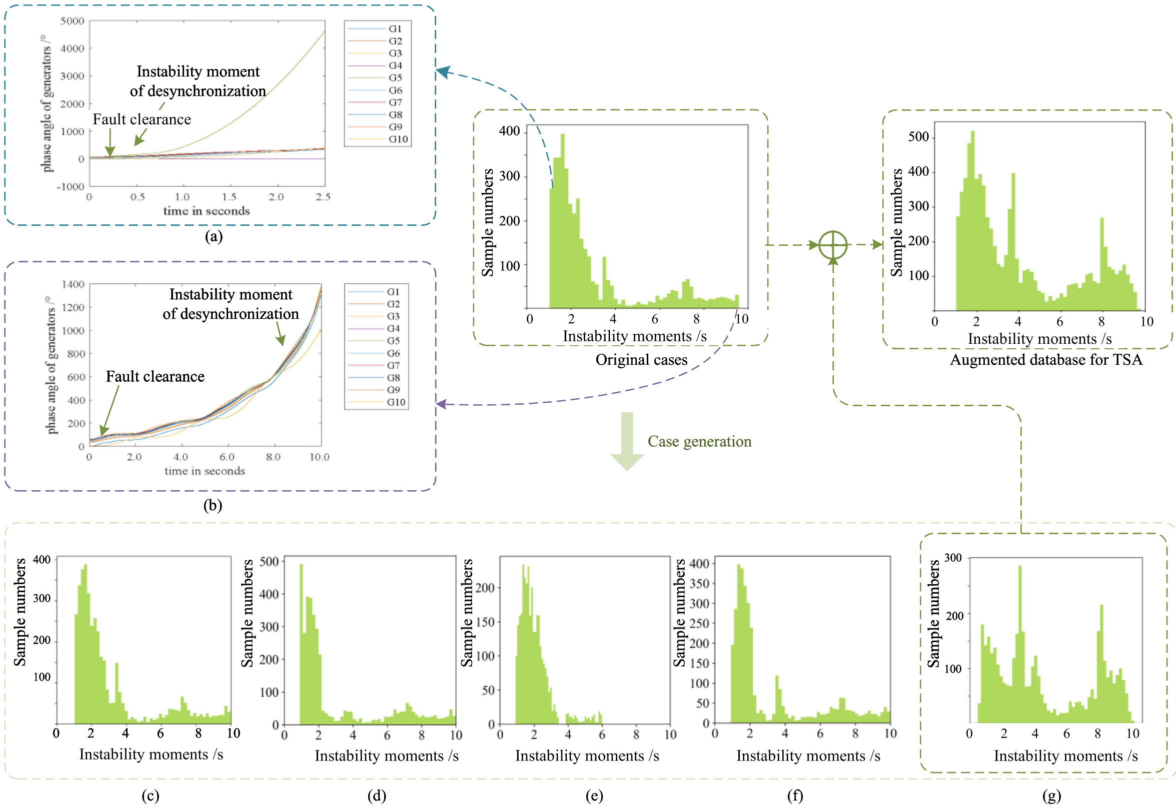

Fig. 4. Comparison of different data augmentation methods. (a) Case of aperiodic instability. (b) Case of oscillatory instability. (c) Generated cases with DCGAN. (d) Generated cases with cGAN. (e) Generated cases with VAE. (f) Generated cases with DDPM. (g) Generated cases with proposed method.

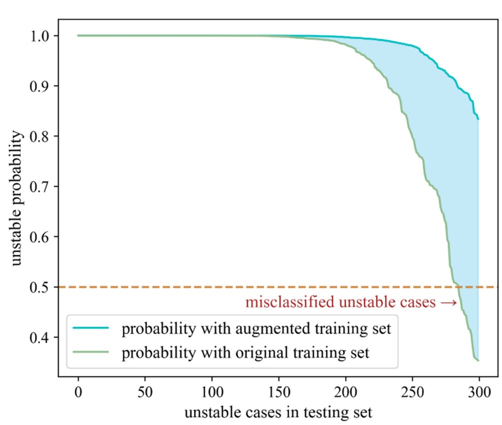

Fig. 5. Visualization of the TSA classifier trained with (a) original data, and (b) augmented data via the proposed model.

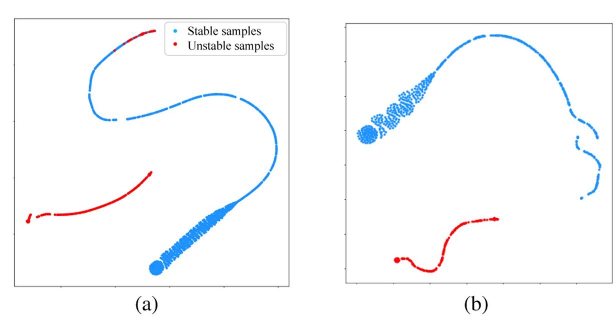

Fig. 6. Visualization of the TSA classifier trained with (a) original data, and (b) augmented data via the proposed model.

softmax function. The prediction is considered more convincing when the output for a specific class is significantly higher than the outputs for the other classes.

Fig. 5 illustrates the probability of the CNN-based TSA classifier for 300 unstable samples in the testing sets. The model trained with the original training set may occasionally misclassify samples due to their subtle instability characteristics at the fault clearance instant, but these samples will be accurately classified by the improved model trained with augmented data. Moreover, the enhanced model generally assigns higher instability probabilities to these samples, suggesting improved performance in recognizing unstable cases. This demonstrates that the proposed data augmentation algorithm produces realistic and diverse instability cases, and the inclusion of the generated data enables the TSA classifier to learn enriched instability characteristics, thus effectively enhancing the TSA performance.

Fig. 6 visualizes the feature representations at the final fully connected layer of the CNN classifier using t-distributed stochastic neighbor embedding (t-SNE) [36]. As shown in Fig. 6(a), a substantial overlap exists between samples of distinct labels, indicating that the classifier struggles to discern stable from unstable instances. However, in Fig. 6(b), the gap between different types of data is enlarged after applying the proposed

TABLE IX
REALISM LEVEL OF GENERATED UNSTABLE SAMPLES

training data	FID (rare)	FID (all)	Average instability moments (s)
Without pollution	0.1900	0.1205	7.23
With pollution	0.1942	0.1478	7.50

TABLE X
ACCURACY OF DIFFERENT TSA CLASSIFIERS WITH DIFFERENT TRAINING DATASETS

Test data	Training data	Classifiers (%)	
		GCN	CNN
Without pollution	Raw data	97.01	96.82
	Augmented data	97.59	97.21
With pollution	Raw data	96.98	96.78
	Augmented data	97.42	97.15

data augmentation method, reinforcing the efficacy of the proposed data augmentation method in improving the TSA task.

V. PERFORMANCE OF PROPOSED METHOD ON THE LARGE-SCALE POWER SYSTEM

To assess the effectiveness of our proposed method in a large-scale power system with limited data, we conducted experiments on the Northeast Power Coordinating Council (NPCC) 48-machine 140-bus system, which simulates the power grids of the Northeastern United States and Canada [37]. Following the database generation structure described in Section III-A, the feature map is defined as $\mathbf{Z} \in \mathbb{R}^{d \times c}$, where d is 3 and c is 48, corresponding to different electrical variables for a total of 48 generators in this power system. In total, 4000 scenarios are generated, including 1548 unstable scenarios with an average instability moment of 3.72 s.

The results in Table IX demonstrate that the proposed method can generate highly realistic instability samples in large-scale power grids, with the average instability moment shifting from 3.72 to 7.50 s. The realism of the generated samples in Table IX is lower than that in Table III, as indicated by higher FID scores. This is due to the smaller data size and increased complexity of the large-scale power system. However, the relatively low FID values in Table IX indicate that the proposed method is still capable of effectively generating realistic samples.

Table X shows that the performance of CNN-based TSA classifier declines for large-scale power grids with limited data, compared to Table VIII. Therefore, we employ a graph convolutional network (GCN) as the TSA classifier to evaluate the effectiveness of the proposed data generation method within a large-scale power grid [38]. The GCN-based classifier is trained with the topological information of the NPCC power grid. As indicated in Table X, the GCN demonstrates superior classification performance compared to CNNs, leveraging the power grid's topological information and effectively capturing spatial relationships. This result further demonstrates the potential of the proposed method in generating data that significantly enhances the performance of various data-driven TSA classifiers.

Furthermore, Fig. 7 visualizes the feature representations at the final layer of the GCN classifier using t-SNE [36]. This visualization indicates that the model trained on the augmented samples has better recognition capabilities for stable and unstable samples compared to the model trained using the original samples. This confirms that the proposed method generates a significant number of unstable data samples that conform to the instability characteristics of the power grid. Consequently, the proposed method is applicable to large power grids and small data scenarios, demonstrating its practical value.

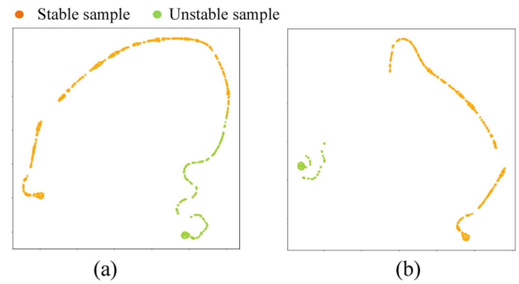

Fig. 7. Visualization of the GCN-based TSA classifier for a large-scale power system trained with (a) original data, and (b) augmented data.

VI. CONCLUSION

Focusing on enhancing the reliability of data-driven TSA in power systems, this article presents a data-driven case generation method to tackle the challenges posed by small sample size and data imbalance. Our proposed case generation method generates realistic and diverse instability samples, which enrich the training database for TSA classifiers. The incorporation of a supervised CNN model into the GAN structure enables the generation of samples with high realism and diversity, thereby altering the long-tailed distribution of the raw dataset. Numerical experiments demonstrated that our proposed framework outperforms existing methods. Finally, the training sets augmented with the proposed method led to significant improvements in online TSA tasks.

REFERENCES

[1] N. G. Baltas et al., "A comparative analysis of decision trees, support vector machines and artificial neural networks for on-line transient stability assessment," in *Proc. Int. Conf. Smart Energy Syst. Technol.*, Seville, Spain, Sep. 2018, pp. 1–6.

[2] F. R. Gomez, A. D. Rajapakse, U. D. Annakkage, and I. T. Fernando, "Support vector machine-based algorithm for post-fault transient stability status prediction using synchronized measurements," *IEEE Trans. Power Syst.*, vol. 26, no. 3, pp. 1474–1483, Aug. 2011.

[3] A. Gupta, G. Gurrala, and P. S. Sastry, "An online power system stability monitoring system using convolutional neural networks," *IEEE Trans. Power Syst.*, vol. 34, no. 2, pp. 864–872, Mar. 2019.

[4] L. Zhu and D. J. Hill, "Data/model jointly driven high-quality case generation for power system dynamic stability assessment," IEEE Trans. Ind. Inform., vol. 18, no. 8, pp. 5055–5066, Aug. 2022.

[5] Y. Tang, Y. Huang, H. Wang, C. Wang, Q. Guo, and W. Yao, "Framework for artificial intelligence analysis in large-scale power grids based on digital simulation," *CSEE J. Power Energy Syst.*, vol. 4, no. 4, pp. 459–468, Dec. 2018.

[6] G. Douzas, F. Bacao, and F. Last, "Improving imbalanced learning through a heuristic oversampling method based on K-means and SMOTE," *Inf. Sci.*, vol. 465, pp. 1–20, 2018.

[7] N. V. Chawla, K. W. Bowyer, L. O. Hall, and W. P. Kegelmeyer, "SMOTE: Synthetic minority over-sampling technique," *J. Artif. Intell. Res.*, vol. 16, pp. 321–357, Jun. 2002.

[8] G. Grdenić, M. Delimar, and J. Beerten, "AC grid model order reduction based on interaction modes identification in converter-based power systems," *IEEE Trans. Power Syst.*, vol. 38, no. 3, pp. 2388–2397, May 2023.

[9] C. Ren and Y. Xu, "A fully data-driven method based on generative adversarial networks for power system dynamic security assessment with missing data," *IEEE Trans. Power Syst.*, vol. 34, no. 6, pp. 5044–5052, Nov. 2019.

[10] R. Yuan, B. Wang, Y. Sun, X. Song, and J. Watada, "Conditional style-based generative adversarial networks for renewable scenario generation," *IEEE Trans. Power Syst.*, vol. 38, no. 2, pp. 1281–1296, Mar. 2023.

[11] Y. Li, Y. Wang, and S. Hu, "Online generative adversary network based measurement recovery in false data injection attacks: A cyber-physical approach," *IEEE Trans. Ind. Inform.*, vol. 16, no. 3, pp. 2031–2043, Mar. 2020.

[12] J. Liu, F. Qu, X. Hong, and H. Zhang, "A small-sample wind turbine fault detection method with synthetic fault data using generative adversarial nets," *IEEE Trans. Ind. Inform.*, vol. 15, no. 7, pp. 3877–3888, Jul. 2019.

[13] J. Li, H. Yang, L. Yan, Z. Li, D. Liu, and Y. Xia, "Data augment using deep convolutional generative adversarial networks for transient stability assessment of power systems," in *Proc. 39th Chin. Control Conf.*, 2020, pp. 6135–6140.

[14] Y. Chen, Y. Wang, D. Kirschen, and B. Zhang, "Model-free renewable scenario generation using generative adversarial networks," *IEEE Trans. Power Syst.*, vol. 33, no. 3, pp. 3265–3275, May 2018.

[15] J. Li, Z. Chen, L. Cheng, and X. Liu, "Energy data generation with Wasserstein deep convolutional generative adversarial networks," *Energy*, vol. 257, 2022, Art. no. 124694.

[16] S. R. Chhetri, A. B. Lopez, J. Wan, and M. A. Al Faruque, "GAN-Sec: Generative adversarial network modeling for the security analysis of cyber-physical production systems," in *Proc. Des. Autom. Test Europe Conf. Exhibit.*, 2019, pp. 770–775.

[17] W. Dong, X. Chen, and Q. Yang, "Data-driven scenario generation of renewable energy production based on controllable generative adversarial networks with interpretability," *Appl. Energy*, vol. 308, 2022, Art. no. 118387.

[18] S. Liu et al., "LOSGAN: Latent optimized stable GAN for intelligent fault diagnosis with limited data in rotating machinery," *Meas. Sci. Technol.*, vol. 32, no. 4, Feb. 2021, Art. no. 045101.

[19] Y. Zhou et al., "A novel data-driven approach for transient stability prediction of power systems considering the operational variability," *Elect. Power Energy Syst.*, vol. 107, pp. 379–394, 2019.

[20] X. Mao, Q. Li, H. Xie, R. Y. K. Lau, Z. Wang, and S. P. Smolley, "Least squares generative adversarial networks," in *Proc. IEEE Int. Conf. Comput. Vis.*, 2017, pp. 2813–2821.

[21] A. Gupta, G. Gurrala, and P. S. Sastry, "Instability prediction in power systems using recurrent neural networks," in *Proc. 26th Int. Joint Conf. Artif. Intell.*, 2017, pp. 1795–1801.

[22] J. Chow and K. Cheung, "A toolbox for power system dynamics and control engineering education and research," *IEEE Trans. Power Syst.*, vol. 7, no. 4, pp. 1559–1564, Nov. 1992.

[23] M. Heusel et al., "GANs trained by a two time-scale update rule converge to a local Nash equilibrium," in *Proc. Int. Conf. Neural Inf. Process. Syst.*, 2017, pp. 6629–6640.

[24] IEEE Standard for Synchrophasor Data Transfer for Power Systems, IEEE Standard C37.118.2-2011 (Revision of IEEE Std C37.118-2005), 2011.

[25] B. Tan et al., "Spatial-temporal adaptive transient stability assessment for power system under missing data," *Int. J. Elect. Power Energy Syst.*, vol. 123, 2020, Art. no. 106237.

[26] D. Ulyanov, A. Vedaldi, and V. Lempitsky, "Instance normalization: The missing ingredient for fast stylization," 2017, arXiv:1607.08022.

[27] B. Xu, N. Wang, T. Chen, and M. Li, "Empirical evaluation of rectified activations in convolutional network," 2015, arXiv:1505.00853.

[28] K. He, X. Zhang, S. Ren, and J. Sun, "Deep residual learning for image recognition," in *Proc. IEEE Conf. Comput. Vision Pattern Recognit.*, 2016, pp. 770–778.

[29] X. Wang, R. Girshick, A. Gupta, and K. He, "Non-local neural networks," in *Proc. IEEE/CVF Conf. Comput. Vision Pattern Recognit.*, 2018, pp. 7794–7803.

[30] F. Z. Okwonu, B. L. Asaju, and F. I. Arunaye, "Breakdown analysis of Pearson correlation coefficient and robust correlation methods," *IOP Conf. Series: Mater. Sci. Eng.*, vol. 917, Sep. 2020, Art. no. 012065.

[31] M. Kang et al., "A cross-modal generative adversarial network for scenarios generation of renewable energy," *IEEE Trans. Power Syst.*, vol. 39, no. 2, pp. 2630–2640, Mar. 2024.

[32] O. Dalmaz et al., "Denoising diffusion adversarial models for unconditional medical image generation," in *Proc. 31st Signal Process. Commun. Appl. Conf.*, 2023, pp. 1–5.

[33] Z. Wan, Y. Zhang, and H. He, "Variational autoencoder based synthetic data generation for imbalanced learning," in *Proc. IEEE Symp. Ser. Comput. Intell.*, 2017, pp. 1–7.

[34] S. Wu et al., "Improved deep belief network and model interpretation method for power system transient stability assessment," *J. Modern Power Syst. Clean Energy*, vol. 8, no. 1, pp. 27–37, Jan. 2020.

[35] T. T. Nguyen et al., "Ensemble selection based on classifier prediction confidence," *Pattern Recognit.*, vol. 100, 2020, Art. no. 107104.

[36] L. van der Maaten and G. Hinton, "Visualizing data using T-SNE," *J. Mach. Learn. Res.*, vol. 9, no. 86, pp. 2579–2605, 2008.

[37] J. Fang, L. Zheng, and C. Liu, "A novel method for missing data reconstruction in smart grid using generative adversarial networks," *IEEE Trans. Ind. Inform.*, vol. 20, no. 3, pp. 4408–4417, Mar. 2024.

[38] J. Hu, Q. Wang, Y. Ye, Z. Wu, and Y. Tang, "A high temporal-spatial resolution power system state estimation method for online DSA," *IEEE Trans. Power Syst.*, vol. 39, no. 1, pp. 877–889, 2024.

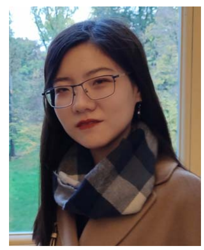

Jiashu Fang (Member,IEEE)received the B.S. degree in electrical engineering from North China Electric Power University, Beijing, China, in 2015, the M.S. degree in electrical power system from University of Manchester, U.K., in 2016, and the Ph.D. degree in electrical engineering from North China Electric Power University, in 22024.

She is currently a Postdoctoral Researcher with the University of Electronic Science and Technology of China, Chengdu, China. Her research interests include applications of machine learning and data science in power systems.

Le Zheng (Member, IEEE) received the B.S. and Ph.D. degrees in electrical engineering from Tsinghua University, Beijing, China, in 2011 and 2017, respectively.

He had been a Postdoctoral Research Fellow with Stanford University, Stanford, CA, USA, from 2017 to 2019. He is currently a Faculty Member with the North China Electric Power University, Beijing, China. His research interests include stability and control of power electronics dominated power systems and renewable energy conversion systems, and machine learning applications in power systems.

Chongru Liu (Senior Member, IEEE) received the B.S. and Ph.D. degrees in electronic engineering from Tsinghua University, Beijing, China, in 2000 and 2006, respectively.

She is currently a Professor, Ph. D. supervisor, and the Dean of Undergraduate Academic Affairs Office, North China Electric Power University, Beijing, China.

Dr. Liu was selected for Beijing Science and Technology Nova Talent Support Plan in 2009, and the Ministry of Education Excellent Talents Support Plan for the New Century in 2012. She is the Standing Director of the Tenth Council of Beijing Electrical Engineering Society, Director of the Committee on Science Popularization and Education, Member of the Fifth and Sixth National Technical Committee on Power System Management and Information Exchange Standardization, Member of the Power System Automation Committee of China Electrical Engineering Society, Member of the Foreign Affairs Committee of China Electrical Engineering Society, and Member of Beijing Science Representatives of the Ninth Congress of the Technical Association.

Chenbo Su received the M.S. and doctoral degrees in electrical engineering from North China Electric Power University, Beijing, China, in 2017 and 2022, respectively.

He is currently an Assistant Researcher with Tsing Hua University, Beijing, China. His research interests include the control and stability analysis of grid-connected new energy and HVdc transmission systems.